*Proceedings of The Fourteenth (2004) International Offshore and Polar Engineering Conference*
*Toulon, France, May 23–28, 2004*

*ISBN 1-880653-62-1 (Set); ISSN 1098-6189 (Set)*

# Numerical Modeling and Experiments for Solitary Wave Shoaling and Breaking over a Sloping Beach

*Stéphan T. Grilli*[1], *Richard W. Gilbert*[1], *Pierre Lubin*[2], *Stéphane Vincent*[2], *Dominique Astruc*[3], *Dominique Legendre*[3], *Marie Duval*[3], *Olivier Kimmoun*[4], *Hubert Branger*[5], *Déborah Devrard*[6], *Philippe Fraunié*[6], *and Stéphane Abadie*[7]

[1]University of Rhode Island (URI), Narragansett, RI, USA

[2]TREFLE-ENSCPB, Pessac, France

[3]Institut de Mécanique des Fluides de Toulouse (IMFT), UMR 5502 CNRS-INPT-UPS, Toulouse, France

[4]Ecole Supérieure d'Ingénieurs de Marseile (ESIM), France

[5]IRPHE, Marseille, France

[6]LSEET, Université de Toulon et du Var, France

[7]LaSAGeC, Université de Pau et des Landes, Anglet, France

## ABSTRACT

This research deals with the validation of fluid dynamic models, used for simulating shoaling and breaking solitary waves on slopes, based on experiments performed at the Ecole Supérieure d'Ingénieurs de Marseille's (ESIM) laboratory. A separate paper, also presented at this conference, reports on experiments. In a first part of this work, a fully nonlinear potential flow model based on a Boundary Element Method (BEM) developed at the University of Rhode Island (URI), is used to generate and propagate solitary waves over a slope, up to overturning, in a set-up closely reproducing the laboratory tank geometry and wavemaker system. The BEM model uses a boundary integral equation method for the solution of governing potential flow equations and an explicit Lagrangian time stepping for time integration. In a second part, several Navier-Stokes (NS) models, developed respectively at TREFLE-ENSCPB, IMFT, IRPHE and LSEET are initialized based on the BEM solution and used for modeling breaking solitary waves in a finely discretized region encompassing the top of the slope and the surfzone. The NS models are based on the Volume of Fluid Method (VOF). This paper mostly deals with the first part, which includes calibration and comparison of BEM results with experiments, for the generation of solitary waves in the physical wave tank. Thus, parameters of the physical wave tank were numerically matched, including tank geometry and motion of the wavemaker paddle corresponding to the generation of solitary waves. Use and coupling of the BEM and VOF models for the simulation of solitary wave breaking is discussed in the paper.

KEYWORDS : Nonlinear nearshore wave transformations, wave shoaling and breaking, numerical wave tank, boundary element method, solitary wave.

## INTRODUCTION

Numerical models based on the Boundary Element Method (BEM), combined to an explicit higher-order Lagrangian time stepping, have proved very efficient and accurate for solving fully nonlinear potential flow (FNPF) equations with a free surface, in two- (2D) and three-dimensions (3D) (e.g., Grilli et al., 1989, 1990, 1996, 2001; Grilli, 1997). When applied to the modeling of surface wave generation and propagation over varying topography, such models have recently been referred to as *Numerical Wave Tanks* (NWT). Due to their simplicity as compared to periodic waves, solitary waves have often been used for both model development and experimental validation. Grilli et al. (1994, 1997ab), for instance, showed that the shape of shoaling and breaking solitary waves over slopes could be simulated within a few percent of experimental measurements in a 2D-BEM-FNPF-NWT. Similar validations were repeated in 3D, e.g., by Grilli et al. (2001). Both potential flow equations and BEM models, however, break down after impact of the breaker jet on the free surface.

Recently, Volume of Fluid (VOF) models solving Navier-Stokes (NS) equations with a free surface have been used to model breaking waves (e.g., Lubin et al., 2003; Vincent and Caltagirone, 2004; Guignard

et al., 2001). Such models, however, are much more computationally intensive than BEM models and suffer from numerical diffusion over long distances of propagation. Hence, a coupled approach has been applied in both 2D and 3D, in which wave generation and shoaling is simulated in a BEM-NWT up to a point close to breaking, and a VOF model is initialized by results of the BEM model over a finely discretized grid covering the upper part of the slope. Wave breaking and post-breaking are then computed in the VOF model (Guignard et al., 1999, Lachaume et al., 2003, Biausser et al., 2003).

This paper reports on the experimental validation of the coupled modeling approach outlined above, for the shoaling and breaking of solitary waves on a slope performed in the precision wave tank of the Ecole Supérieure d'Ingénieurs de Marseille (ESIM). Details of ESIM's laboratory experiments can be found in Kimmoun et al. (2004). Waves were generated in the laboratory using a flap wavemaker whose axis of rotation was located below the tank bottom (Fig. 1). Experiments were run over a range of water depths and for two different wave sizes, referred to as type 2 for a larger solitary wave, and type 7 for a smaller solitary wave. Experimental data includes wave elevation measured at 6 wave gages (S1 to S6 in Fig. 1), visualizations of breaking wave shapes around the location of the shallower probe over the slope, and flow velocities measured in the breaking wave area using a Particle Image Velocimetry (PIV) method. The latter represents a significant improvement as compared to most earlier work reported to date, which was usually devoted to comparing measured and computed wave shape (e.g., Grilli et al., 1994, 1997ab; Guignard et al., 1999).

## NUMERICAL MODEL

The 2D BEM model developed by Grilli et al. (1989,1990,1996) is used in these simulations. The model approximates arbitrary wave tank boundary geometry as a series of nodes, and uses 2 to 5 node isoparametric or cubic spline boundary elements for interpolating in between the nodes. The BEM solution for the flow kinematics and pressure is computed as a function of time at boundary nodes. Surface piercing numerical wave gages can be specified, at which computed free surface elevation are recordedover time. Similarly, the model can provide the BEM solution at a specified distribution of (internal) points within the domain (e.g., Grilli and Subramanya, 1996; Guignard at al., 1999; Lachaume et al., 2003). These points can be defined either on a fixed grid or on vertical lines, for a number of variable intervals between the free surface and the bottom boundaries. Velocity and pressure computed at such internal points are used to initialize the VOF models, as detailed in Guignard et al. (1999) and Lachaume et al. (2003).

The BEM model included various methods of wave generation (e.g., Grilli, 1997). However, it did not include a method that exactly matched wave generation in physical experiments. Hence, the same type of flap wavemaker as used in experiments was implemented in the model, including the curved boundary at the base of the paddle (Fig. 1), with its kinematics specified based on the same algorithm as used for operating the laboratory paddle hydraulic jack. This algorithm calculates the angle of the paddle as a function of time and converts this angle $\theta(t)$ to the horizontal jack position. ESIM's algorithm was based on using a constant time step. The BEM model uses a varying time step (adjusted based on a Courant condition at each step; Grilli and Subramanya, 1996), which required changing the generation algorithm to produce the same motion using the varying time step. Changes also included computation of paddle angular velocity $\theta'$ and acceleration $\theta''$, which are needed for BEM boundary conditions (see, e.g., Grilli, 1997 for detail). Figs. 2 and 3 show variations of $\theta$, $\theta'$, and $\theta''$ as a function of time, used for generating

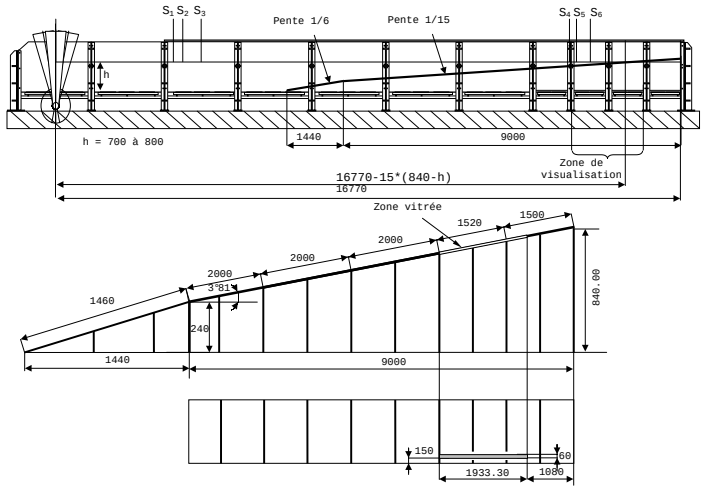


Fig. 1 : Sketch of ESIM's physical wave tank.

the two types of solitary waves tested in experiments and modeled in the NWT.

In numerical simulations, the tank geometry, particularly the bottom variation made of 1:6 and 1:15 plane slopes, was specified to match the experimental tank geometry. Numerical wave gages were located in the NWT at the same locations as in the laboratory tank, to record computed surface elevations. Initial computations were performed using the same paddle kinematics, i.e., $\theta(t)$, as the commands generated and sent to the paddle in the physical tank. However, discrepancies between the numerical and physical data were observed at initial gages (S1-S3) and the generation algorithm was subsequently adjusted to better approximate the solitary wave generated in experiments. This *NWT calibration* stage is detailed in the following.

### NWT calibration

The parameters of the wavemaker motion algorithm used by ESIM are a wave height parameter $\zeta$, and an empirical adjustment factor $\mu$. For both type 2 and type 7 solitary waves we used $\zeta = 0.4$, with $\mu = 1$ for the type 2 wave, and $\mu = 2$ for the type 7 wave. With these parameters, in the experiments, the generated type 7 wave is about $H = 0.10$ m high in depth $h = 0.74$ m ($H/h = 0.135$), and the type 2 wave is about $H = 0.16$ m high in water of depth $h = 0.76$ m ($H/h = 0.211$). When running numerical simulations with these parameters, significant differences in incident wave heights were observed. Possible reasons for these discrepancies are discussed in the following. Hence, values of the above parameters were adjusted to create incident waves in the model in better agreement with the physical data. After adjustment, wave elevations computed at the first three gages S1-S3 were found in fairly good agreement with experiments, as shown in (top) Figs. 4 and 5. In addition, waves near the breaking point also agreed well with experiments, as shown in (bottom) Figs. 4 and 5 for results at gages S4-S6 (Fig. 1). [Note, gage S5 in experiments seems to produce abnormal results, maybe due to a faulty calibration.]

In computations, relative errors on mass conservation in the NWT were on the order of $10^{-8}$ for any given time step, and errors on initial NWT volume conservation were less than 0.05% over the entire simulations, for all cases. Such small errors suggest both an accurate BEM solution and specification of the paddle motion as boundary condition in the numerical model.

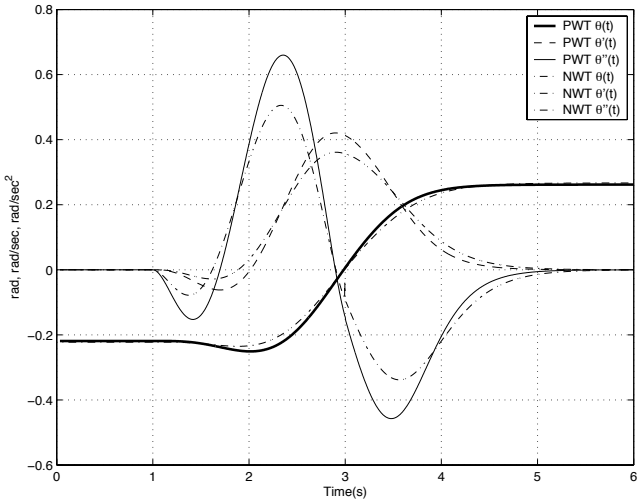


Fig. 2 : *Solitary wave Type 7.* Comparison of Physical Wave Tank(PWT) paddle input and Numerical Wave Tank (NWT) paddle input to create similar waves.

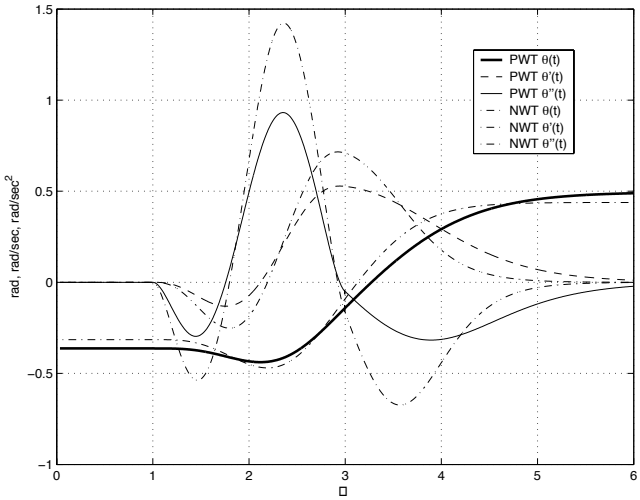


Fig. 3 : *Solitary wave Type 2.* Comparison of Physical Wave Tank (PWT) paddle input and Numerical Wave Tank (NWT) paddle input to create similar waves.

## Discussion of discrepancies

**Paddle motion** There was no feedback measurement of the paddle motion in experiments. Doing a sensitivity analysis, we found that small changes in paddle motion with respect to the output of ESIM's generation algorithm could produce significantly different results in generated waves. Fig. 2, for instance, shows for solitary wave for type 7 differences between the physical wave tank paddle angle variation as a function of time specified in ESIM's algorithm, and that eventually used in the NWT, after adjustment were made to match the experimental incident wave height in the specified water depth. Variations of angular velocity and acceleration are also shown. When used in the NWT, these two angular variations produced waves that differed in height by about 20%, while differences in paddle angular motion are quite small. Hence, if the actual motion of the paddle in the experimental tank varied by an amount as small as shown on the figure, there would be a significant wave height difference. Thus, without measurement of the actual physical paddle mo-

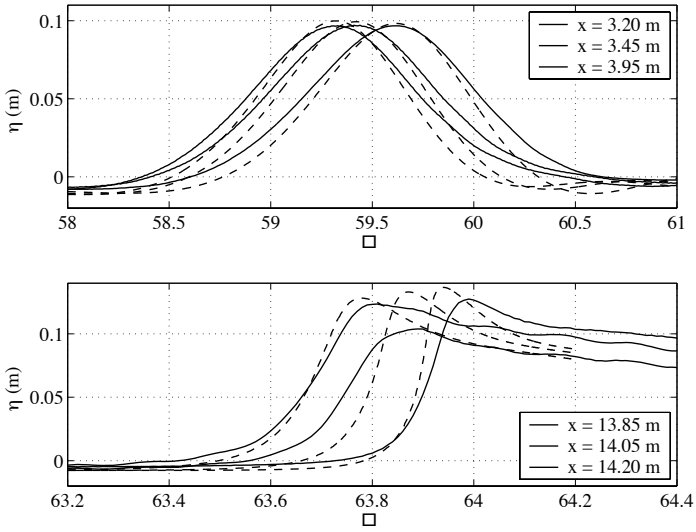


Fig. 4 : *Solitary wave Type 7.* Comparison of experimental data (— —-) and NWT simulations (- - - - -) at wave gages (as a function of time (Fig. 1): S1 ($x$ =3.20 m); S2 ($x$ =3.45 m); S3 ($x$ =3.95 m); S4 ($x$ =13.85 m); S5 ($x$ =14.05 m); and S6 ($x$ =14.20 m). The initial water depth is $h = 0.74$ m.

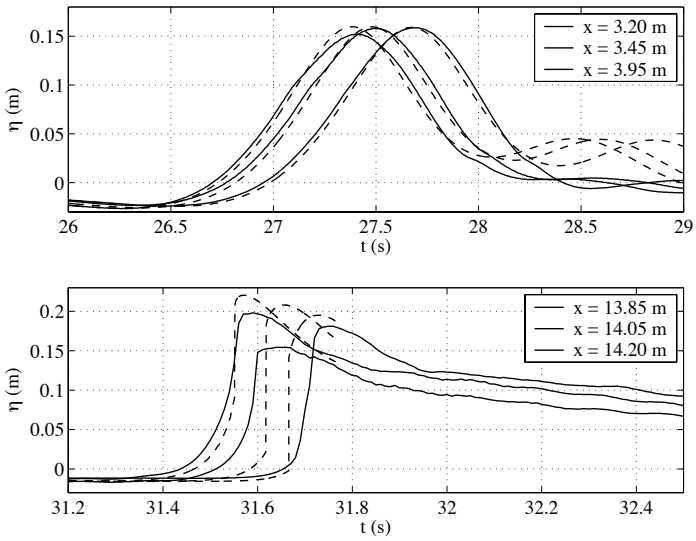


Fig. 5 : *Solitary wave Type 2.* Same definitions as in Fig. 4. The initial water depth is $h = 0.76$ m.

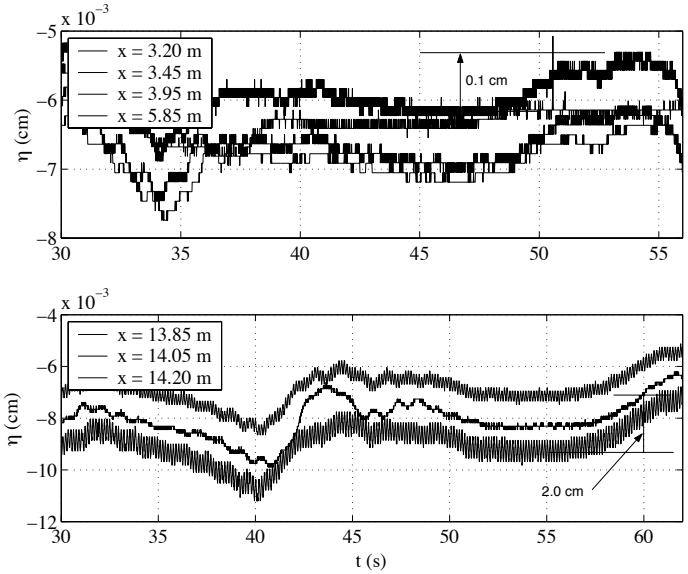


Fig. 6 : *Solitary wave Type 7.* Surface elevations measured at wave gages S1-S6 (see Fig. 4 for definition) in the physical wave tank, prior to wave generation, during paddle pullback, in initial water depth $h = 0.7$ m.

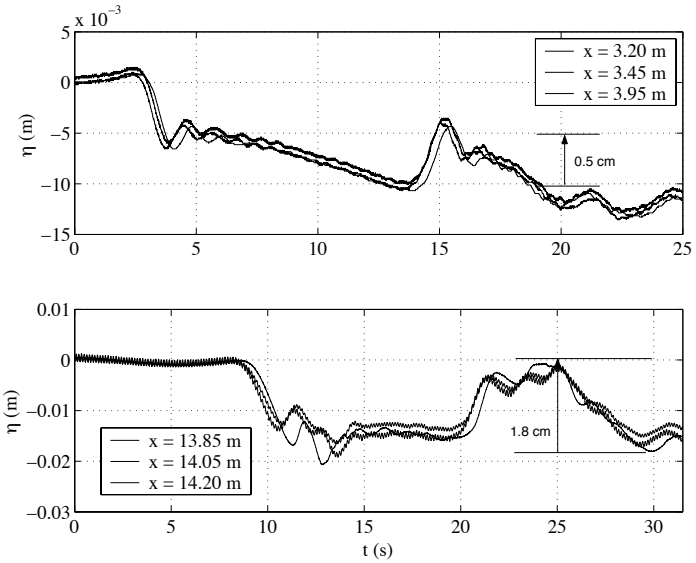


Fig. 7 : *Solitary wave Type 2.* Surface elevations measured at wave gages S1-S6 (see Fig. 4 for definition) in the physical wave tank, prior to wave generation, during paddle pullback, in initial water depth $h = 0.72$ m.

tion, it becomes difficult to verify how closely the numerical model can simulate the physical experiment, unless the NWT paddle motion parameters were adjusted to better match incident waves at gages S1-S3, as was done here. The paddle motion was adjusted by slightly changing values of parameters $\zeta$ and $\mu$.

This is even more apparent on Fig. 5, which shows the (larger) differences between the physical and numerical paddle motions required to match incident wave heights for type 2 solitary waves. Such large differences were required because the physical paddle motion, when specified in the NWT, created wave heights around 80% higher in the numerical model than in experiments.

Additional uncertainty in wave generation is also due to small leakage occurring past each side of the physical paddle as it moves through the generation arc. Thus, larger waves will cause more pressure against the paddle, which will cause a greater amount of leakage past the paddle. This is also well supported by observations.

**Initial paddle pullback** At the start of the physical experiments, the paddle begins at the vertical position and, over about 20 to 50 seconds, is slowly drawn back to its start position before the wave is generated (see negative initial angle in Figs. 2 and 3). Fig. 6 shows that this slow motion results in a slow (7 second period) oscillation, of about 0.3 cm amplitude, at the wave gages located at the far end of the tank, type 7 wave, and Fig. 7 shows a similar 5 second period oscillation of up to 2 cm amplitude for the type 2 wave. By contrast, wave gages located closer to the paddle demonstrate very little oscillation, less than 0.5 cm, in both cases.

It should be noted that numerical simulations start at the beginning of the paddle impulsive motion causing wave generation. To reduce discrepancies, in the NWT, the initial water depth was approximated to match the average depth measured in the physical tank right after pullback of the paddle from vertical, which is smaller than the initial depth.

**Other sources of discrepancies** The NWT calculations are based on the assumption of an inviscid irrotational fluid, and therefore do not include any internal dissipation or friction losses. A reduction in wave height in the physical tank, however, could also occur because of viscous friction along the bottom and sidewalls. Such effects should be relatively more significant for long waves like solitary waves, for which horizontal particle velocities remain large down to the bottom. An initial (rough) calculation of these effects at ESIM's experiments, however, suggests that only a 2% or less loss in wave kinetic energy would be caused by friction effects, which could not account for the observed differences in wave height. This is in agreement with similar earlier experiments, which showed that, prior to breaking, viscous losses are negligible for shoaling solitary waves (e.g., Grilli et al., 1994, 1997).

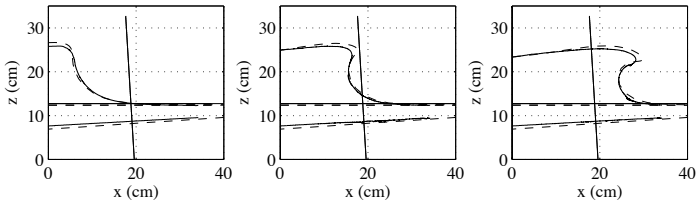


Fig. 8 : *Solitary wave Type 7.* Comparison of breaker visualization (— —) with numerical wave profile (- - - - -), in depth $h = 0.72$ m.

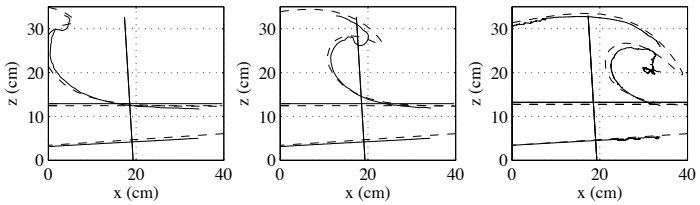


Fig. 9 : *Solitary wave Type 2.* Comparison of breaker visualization (— —) with numerical wave profile (- - - - -), in depth $h = 0.72$ m. Note spilling at crest of breaker in physical model.

## Comparison based on the revised generation

After adjustment of the paddle parameters in the NWT, incident waves and waves close to breaking are found to be in good agreement with experiments. This is confirmed in Figs. 8 and 9 which also show relatively small differences in the breaker shape visualized around the location of gage S6, for both types of waves. There is a very good correlation between the physical and numerical results based on the breaker shapes observed.

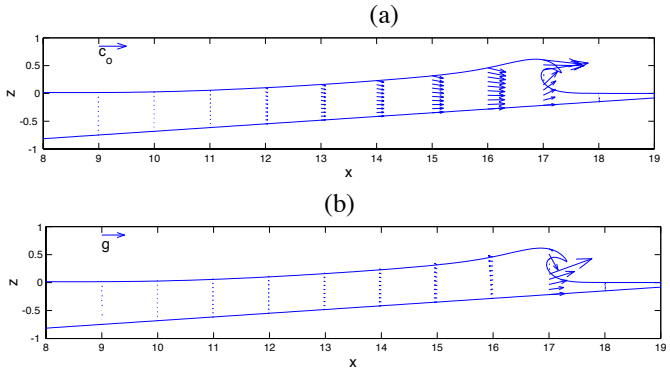


Fig. 10 : Example of internal (a) velocity and (b) acceleration field generated for a solitary wave with incident height $H/h = 0.6$ shoaling up a 1:15 slope, in the BEM-NWT. Results have been scaled by depth, $c_o$ indicates the magnitude of the wave celerity in the constant depth area, and $g$ the gravitational acceleration.

# MODELING OF BREAKING AND POST-BREAKING WAVES

## Coupling of BEM and VOF NWTs

Now that the BEM-NWT has been shown to fairly well reproduce experimental conditions in the breaking wave area (e.g., Figs. 8 and 9), the model can be used to initialize VOF computations in the upper slope region of the NWT, over a fine spatial horizontal and vertical grid. This requires values of velocity $\boldsymbol{u} = (u, w)$ and pressure $p$ at the grid cell centers. Such results can be computed explicitly in the BEM-NWT as a function of the boundary solution, at any time step. Fig. 10, for instance, illustrates this by showing velocity and total acceleration fields computed at breaking for a solitary wave, with incident height $H/h = 0.6$, shoaling up a 1:15 slope. We see that, during wave overturning, maximum horizontal velocity reaches up to $3c_o$ and acceleration of about $3g$ within the breaker jet.

Similar results will be obtained for Solitary wave types 2 and 7 over VOF grids corresponding to the different models being tested, and used to carry out VOF modeling, as explained in the following. Results will be presented during the conference.

Various numerical implementations of the NS-VOF equations, were used in the series of models used in this work, for validation based on results of both these experiments and BEM-NWT modeling. Guignard et al. (1999,2001) and Lachaume et al. (2003), for instance, used the LSEET VOF model, which is based on a two-fluid model and the pseudo-compressibility method. The free surface is interpolated by piecewise linear segments. Below, as an example, we detail the single fluid VOF model equations used in the TREFLE-ENSCPB model is given in the following (see also, Vincent et al., 1999, 2000). Another VOF method without interface reconstruction was developped at IMFT and already used to study periodic Stokes waves, as well as solitary wave, breaking (Duval et al., 2004). More details will be provided during the conference.

## Single fluid formulation of Navier-Stokes equations

Let us consider the wave propagation problem as a two-phase flow involving a liquid phase (water) and a gaseous phase (air), in a two-dimensional domain in the vertical plane.

A general NS model for multiple fluids is designed by convolving the incompressible NS equations in each fluid and the jump conditions across the interface, by an indicator function $C$ (the "color function"), and by filtering the resulting set of equations using a volume integral operator. Function $C$ characterizes the fraction of one of the fluids, water for example, taking the value 1 in regions filled with water and 0 in regions devoid of water. The air fraction is directly obtained as the complementary $1 - C$ of the water fraction. Assuming the interface between both fluids marks the discontinuity of the indicator function, one can then locate it by finding the $C = 0.5$ isoline.

Several correlation terms are discarded when one uses a single fluid model. Slip between the phases is assumed to be negligible at the free surface and no phase change occurs. The corresponding free surface flow has a continuous velocity field through the free surface and locally conserves mass.

Let $\boldsymbol{u}$ be the velocity field, $\boldsymbol{g}$ the gravity vector, $p$ the pressure, $\sigma$ the surface tension coefficient, $\kappa$ the free surface curvature, $\mu$ the fluid dynamic viscosity, and $\rho$ the fluid density. In a uniform Cartesian coordinate system $(x, z)$, associated with a bounded domain $\Omega$, equations for the single-fluid model can be expressed as follows,

$$\mu = \mu_1,\ \rho = \rho_1 \qquad \text{for } C > 0.5 \tag{1}$$

$$\mu = \mu_0,\ \rho = \rho_0 \qquad \text{for } C \leq 0.5 \tag{2}$$

$$\boldsymbol{\nabla} \cdot \boldsymbol{u} = 0 \tag{3}$$

$$\begin{aligned} \frac{\partial \boldsymbol{u}}{\partial t} \;+\; & (\boldsymbol{u} \cdot \boldsymbol{\nabla})\boldsymbol{u} \;=\; \boldsymbol{g} - \frac{1}{\rho}\boldsymbol{\nabla} p \\ & + \;\frac{1}{\rho}\boldsymbol{\nabla} \cdot \left[\mu\left(\boldsymbol{\nabla}\boldsymbol{u} + \boldsymbol{\nabla}^T\boldsymbol{u}\right)\right] + \frac{\sigma}{\rho}\,\kappa\,\delta_i\,\boldsymbol{n}_i \end{aligned} \tag{4}$$

$$\frac{\partial C}{\partial t} \;+\; \boldsymbol{u} \cdot \boldsymbol{\nabla} C = 0 \tag{5}$$

where $\delta_i$ is a Dirac function denoting the interface, $\boldsymbol{n}_i$ is the unit normal vector to the interface and $\rho_0$, $\rho_1$, $\mu_0$ and $\mu_1$ are the respective densities and viscosities of each fluid phase, respectively. Equations (1) and (2) imply that the physical fluids characteristics are discontinuously modeled. However, this method leads to a less (numerically) diffusive discretized model than the more classically ones using linear formulations.

The time evolution of both the free surface and the fluid physical characteristics is expressed by Eqs. (4 - 5), assuming Eqs. (1 - 3) are verified at all times. Thus, the free surface flow is analysed in terms of an equivalent single fluid whose variable properties $\rho$ and $\mu$ are related to $\rho_0$, $\rho_1$, $\mu_0$ and $\mu_1$ of the two actual fluid phases by the color function C.

## Numerical methods

**Interface capturing method and surface tension discretisation** An interface capturing method, the explicit Lax-Wendroff TVD (LWT) time-stepping scheme, is used for solving the advection equation (5) for the

discontinuous indicator function $C$, after reformulating it using a smooth function (see, Vincent and Caltagirone, 1999 and 2000). This approach allows us to accurately solve free-surface flows inducing strong tearing and stretching of the interface, such that will be occurring during wave breaking.

Due to the volumetric representation, the geometrical properties of the interface, i.e., $\kappa$, $\delta_i$ and $n_i$ are not directly accessible. To avoid explicitly calculating the free surface properties, these are modeled as a function of the volume fraction $C$. In addition, the Continuum Surface Force (CSF) method of Brackbill et al (1992) is used to model the surface tension acting in the NS equations (4).

**Navier-Stokes solver** A Finite-Volume method is applied to discretize the NS equations (3-4) on a staggered grid, and an augmented Lagrangian technique is used to uncouple the pressure and velocity terms in these equations.

The time discretisation of NS equations is achieved through a second-order Euler scheme, or GEAR scheme, on the time derivatives while a second order Hybrid Centered-Upwind scheme is devoted to the non-linear convective terms and a second-order centered scheme is used for the approximation of the viscous and of the augmented Lagrangian terms. The linear system resulting from this implicit discretization is solved with an iterative Bi-Conjugate Gradient Stabilized algorithm, preconditioned using a Modified and Incomplete LU algorithm. All the references concerning the numerical methods can be found in Vincent and Caltagirone (1999 and 2000).

## CONCLUSIONS

We perform an experimental validation of various numerical models for the shoaling and breaking of solitary waves on slopes, based on laboratory experiments performed at ESIM, Marseille, France.

Wavemaker geometry and paddle motion of the physical wave tank, provided for a constant time step, were specified in a numerical BEM-NWT based on FNPF equations and simulations were performed using a varying time step. In order to better match the measured incident waves, the wave generation parameters had to be slightly adjusted in the model, as compared to experiments. This may be due to a number of uncertainties in the physical wave generation method and mechanical systems, which are discussed above.

At this time we have been able to create good numerical simulations of the physical wave experiments using the BEM-NWT, up to overturning of the waves, with a good agreement of both incident wave shapes and of breaking wave profiles. Confirmation of these results will be extended to the comparison of internal velocities generated numerically and measured using the PIV methodm, in ESIM's Physical Wave Tank (see, Kimmoun et al., 2004).

In addition to the work discussed here, the boundary shape and internal velocity and pressure fields prior to breaking will be computed for selected exeprimental test cases, and used as initial conditions for a variety of NS-VOF models. These models will be able to simulate wave breaking and post-breaking and allow for a comparison with corresponding experimental results. This phase of the work is ongoing and results will be reported on during the conference.

## REFERENCES


Biausser, B., Grilli, S.T. and P., Fraunie (2003). "Numerical Simulations of Three-dimensional Wave Breaking by Coupling of a VOF Method and A Boundary Element Method," *Proc. 13th Offshore and Polar Engng. Conf.* (ISOPE03, Honolulu, USA, May 2003), pp 333-339.

Duval, M., Astruc, D. and D., Legendre (2004). "Two-phase Flow Modeling of Breaking Waves Without Interface Reconstruction," *Proc. 14th Offshore and Polar Engng. Conf.* (ISOPE04, Toulon, France, May 2004).

Grilli, S.T., Guyenne, P. and Dias, F. (2001). "A Fully Nonlinear Model for Three-dimensional Overturning Waves Over Arbitrary Bottom," *Int. J. for Numerical Methods in Fluids*, Vol 35, No 7, pp 829-867.

Grilli, S.T., Skourup, J. and I.A., Svendsen (1989). "An Efficient Boundary Element Method for Nonlinear Water Waves," *Engng. Analysis with Boundary Elements,* Vol 6, No 2, pp 97-107.

Grilli, S.T. and Svendsen, I.A. (1990). "Corner Problems and Global Accuracy in the Boundary Element Solution of Nonlinear Wave Flows," *Engng. Analysis with Boundary Elements,* Vol 7, No 4, pp 178-195.

Brackbill, J.U., Kothe, B. D., and C. Zemach (1992) "A Continuum Method for Modeling Surface Tension," *J. Comput. Phys.,* Vol 100, pp 335-354.

Grilli, S.T., Subramanya, R., Svendsen, I.A. and J., Veeramony (1994). "Shoaling of Solitary Waves on Plane Beaches," *J. Waterway Port Coastal and Ocean Engng.,* Vol 120, No 6, pp 609-628.

Grilli, S.T. and R., Subramanya (1996). "Numerical Modeling of Wave Breaking Induced by Fixed or Moving Boundaries," *Computational Mech.,* Vol 17, pp 374-391.

Grilli, S.T. (1997). "Fully Nonlinear Potential Flow Models used for Long Wave Runup Prediction," Chapter in Long-Wave Runup Models, (eds. H. Yeh, P. Liu, and C. Synolakis), pp 116-180. World Scientific Pub.

Grilli, S.T., Svendsen, I.A. and R., Subramanya (1997a). "Breaking Criterion and Characteristics for Solitary Waves on Slopes," *J. Waterway Port Coastal and Ocean Engng.,* Vol 123, No 3, pp 102-112.

Grilli, S.T., Svendsen, I.A. and R., Subramanya (1997b). "Closure of : Breaking criterion and characteristics for solitary waves on slopes," *J. Waterway Port Coastal and Ocean Engng.,* Vol 124, No 6, pp 333-335.

Guignard, S., Grilli, S.T., Marcer, R. and Rey, V. (1999). "Computation of Shoaling and Breaking Waves in Nearshore Areas by the Coupling of BEM and VOF Methods," *Proc. 9th Offshore and Polar Engng. Conf.* (ISOPE99, Brest, France, May 1999), Vol 3, pp 304-309.

Guignard, S., Marcer, R., Rey, V., Kharif, Ch., and Ph. Fraunié (2001). "Solitary Wave Breaking on Sloping Beaches : 2D two-phase Flow Numerical Simulation by SL-VOF Method," *Eur. J. Mech. B-Fluids,* Vol 20, pp 57-74.

Kimmoun, O., Branger, H. and Zucchini, B. (2004). "Laboratory PIV Measurements of Wave Breaking on a Beach," *Proc. 14th Offshore and Polar Engng. Conf.* (ISOPE04, Toulon, France, May 2004).

Lubin, P., Vincent, S., Caltagirone, J.-P. and Abadie, S. (2003). "Fully Three-dimensional Direct Numerical Simulation of Plunging Breaking Waves", *C. R. Mécanique*, Vol 331, pp 495-501.

Vincent, S. and J.P. Caltagirone (1999). "Efficient Solving Method for Unsteady Incompressible Interfacial Flow Problems," *Int. J. Numer. Meth. Fluids*, Vol 30, pp 795-811.

Vincent, S. and J.P. Caltagirone (2000). "A One Cell Local Multigrid Method for Solving Unsteady Incompressible Multi-phase Flows," *J. Comput. Phys.*, Vol 163, pp 172-215.

Vincent, S., Caltagirone, J.-P., Lubin, P., Randrianarivelo, T. N. (2004). "An adaptative Augmented Lagrangian Method for Three-dimensional Multi-material Flows", *Comp. Fluids* (in press).

Lachaume, C., Biausser, B., Grilli, S.T., Fraunie, P. and Guignard, S. (2003). ''Modeling of Breaking and Post-breaking Waves on Slopes by Coupling of BEM and VOF methods," *Proc. 13th Offshore and Polar Engng. Conf.* (ISOPE03, Honolulu, USA, May 2003), pp 353-359.

## ACKNOWLEDGEMENT

This research was supported by the "Programme Atmosphère et Océan à Moyenne Echelle" (PATOM) of the French CNRS, and the University of Rhode Island.